Int J Fract (2018) 214:17–28
https://doi.org/10.1007/s10704-018-0314-7

ORIGINAL PAPER

Dynamic energy release rate evaluation of rapid crack propagation in discrete element analysis

Arthur Coré · Jean-Benoît Kopp · Jérémie Girardot · Philippe Viot

Received: 30 August 2017 / Accepted: 15 September 2018 / Published online: 21 September 2018

Abstract A numerical procedure for estimating the critical dynamic energy release rate (G_{IDc}), based on experimental data is proposed. A generation phase simulation is conducted where fracture parameters can be determined using an experimentally measured crack propagation history (position of the crack tip as a function of time). The discrete element method is used to simulate the dynamic fracture by implementing a node release technique at the crack tip. The results are compared with analytical data on the dynamic propagation of a crack in a semi infinite plate. It reveals that the node release technique causes dynamic instabilities that can only be corrected by adding numerical damping on the edges of the crack or in the entire sample. On the other hand, the progressive node release technique, based on an elasto-damage zone model does not generate dynamic instabilities. It is shown that for a linear relaxation scheme and a damage zone length equal to the mean radius of the discrete elements, results comparable to finite element or analytical methods are obtained in plate structure. The present model offers an alternative to the finite element method to simulate self-similar or more complex crack growth. It also gives a first proper analysis of the evaluation of the critical dynamic energy release rate in a lattice-discrete model.

Keywords Dynamic fracture · Discrete element method · Energy release rate · Node release technique

A. Coré (✉) · J.-B. Kopp · J. Girardot · P. Viot
Arts et Métiers ParisTech, CNRS, I2M Bordeaux, Esplanade des Arts et Métiers, 33400 Talence, France
e-mail: arthur.core@live.fr

J.-B. Kopp
e-mail: jean-benoit.kopp@ensam.eu

J. Girardot
e-mail: jeremie.girardot@ensam.eu

P. Viot
e-mail: philippe.viot@ensam.eu

1 Introduction

RCP (Rapid Crack Propagation) refers to a catastrophic failure of the material where the crack propagates dynamically. The crack tip velocity is in the same order of magnitude than the speed of sound in the material and inertia effects can't be neglected. Simulating the dynamic fracture in a solid is a difficult matter since robust criteria are necessary. Two ways are classically investigated: the *application phase simulation* where the crack propagates automatically and the *generation phase simulation* where the crack propagates manually (Nishioka 1997). The first one is most commonly used. It consists of simulating the propagation of a crack without knowing the crack path history (position of the crack tip at a function of time). The Finite Element Method (FEM) mostly used involves several techniques: element erosion (Song et al. 2008), adaptive meshing (Swenson and Ingraffea 1988), cohesive zones (Zhou et al. 2005) or the Extended FEM (XFEM) (Réthoré 2005; Grégoire 2008; Nistor 2005; Brabel 2007; Menouillard 2007).

The discrete element method (DEM) (also called beam-particle method) offers an alternative to the FEM by allowing a natural propagation of the crack in brittle material generally isotropic (Hedjazi et al. 2012; André et al. 2013; Egholm 2007; Oliver-Leblond et al. 2015; Vassaux et al. 2016; Guessasma and Fortin 2011; Masurel 2015) which can also deal with localization (Delaplace and Ibrahimbegovic 2003) and/or anisotropy (Delaplace and Desmorat 2008). All the works in the literature using the DEM take the benefits of the discrete nature of the geometric domain so that the propagation of a crack is simply described by removing the cohesive links between the elements.

Whether in FEM or DEM, the difficulty lies in finding the right "stress" or "energy" failure criterion that will drive the crack initiation and propagation. That is why the aim of the *generation phase simulation* is to estimate fracture parameters such as the stress intensity factor or the critical energy release rate. These parameters will be useful in the *application phase simulation* to predict the crack propagation (Yanagimoto et al. 2018). The crack path history is experimentally measured and is then used as input data for the numerical model. The numerical sample is loaded in the same way as for the experimental test just before the crack initiation. The sample is then automatically cracked according to the crack path history. The stress or the deformation state of the material near the crack tip can be measured and are the output of the simulation.

The *generation phase simulation* was validated in FEM for the dynamic propagation of crack in plate structures (Kobayashi et al. 1976; Yagawa et al. 1977) or more recently in polymer pipe structures (Kopp et al. 2014a, 2018). Dynamic fracture can also be studied on metallic materials when brittle fracture is observed (Kawabata et al. 2018). These models made it possible to estimate the dynamic energy released rate by dissociating the structural (i.e kinetic energy) response and the materiel effect. The use of the *generation phase simulation* could prevent to underestimate the mechanical properties of materials. Rapid crack propagation being one of the most feared phenomena in engineering problems good fracture criterion are essential.

A review of the dynamic fracture in FEM was issued (Nishioka 1997) and three numerical methods were presented to describe the opening of the crack tip:

Gradual nodal relaxation: The force holding the nodes at the boundaries are progressively reduced with the crack advance (Keegstra et al. 1978; Yagawa et al. 1977);

Cohesive zone model: Cohesive elements are inserted along the crack path. Their mechanical properties are altered when the crack is moving. Their density (Kannan et al. 1993) or their rigidity (Hsu and Zhai 1984; Kostylev and Margolin 1990) are reduced;

Moving element procedure: An adaptive meshing is set up, the node at the crack tip is moving with the crack propagation (Nishioka and Atluri 1980, 1982, 1984; Nishioka 1995).

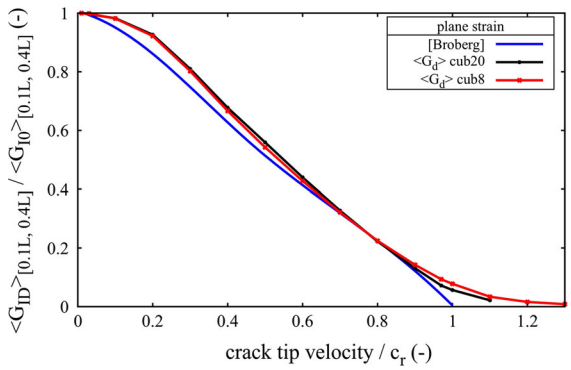

Fig. 1 Dynamic correction factor for a semi-infinite plate: analytical and FEM results (Kopp et al. 2014b)

To validate the crack tip opening methods, numerical results are compared to analytical ones. It has been shown that the higher the crack tip velocity is, the less the energy release rate is. In a crack propagation in a semi-infinite plate in mode I, the critical dynamic energy release rate decreases quasi-linearly (with the increase of the crack tip velocity between $0\,c_r$ and $1\,c_r$ with c_r the Rayleigh wave speed of the material) (Broberg 1960). Figure 1 presents the results in term of the dynamic correction factor (G_{ID}/G_{I0}), analytical and FEM results are compared to eight- and twenty-node cube elements (Kopp et al. 2014b). The dynamic energy release rate G_{ID} represents the energy released to the material during the RCP. The quasi-static energy release rate G_{I0} is computed considering that an increase in crack length Δa corresponds to an elastic unloading of a zone ahead of the crack tip of equivalent length Δa.

In the present work, The DEM is chosen to perform the dynamic fracture by using an elasto-damage zone model similar to the cohesive zone model. Compared

to FEM, DEM needs no re-meshing for various crack paths and is useful for complex geometries. In order to use the DEM for the *application phase simulation*, it is proposed in this paper to validate the DEM for the *generation phase simulation*.

A simple node release technique is first suggested: the crack is simulated by simply deactivating the cohesive links along the crack path one by one. A second technique, called the progressive release technique, is then performed.

2 Methodology

2.1 The discrete element method

The DEM was originally developed for granular assemblies (Cundall and Strack 1979) but its applications have been expanded these last years to other areas such as tribology (Fillot et al. 2007), fluid mechanics (Jalali and Hyppänen 2015) and continuum mechanics (Fakhimi and Villegas 2007). The GranOO workbench (Andre et al. 2014; Gra), developed at I2M (Bordeaux, France) is naturally chosen. GranOO is a collection of C++ libraries and tools that permit to build specific 3D DEM simulations (More details can be found on www.granoo.org). GranOO is based on an explicit time integration scheme (velocity Verlet scheme) (Rougier et al. 2004) which permits a reasonable computational cost for dynamic simulations. Equations for the positions and the velocities of the discrete elements are presented here:

$$\mathbf{p}(t+dt) = \mathbf{p}(t) + dt\,\dot{\mathbf{p}} + \frac{dt^2}{2}\ddot{\mathbf{p}}(t), \tag{1}$$

$$\dot{\mathbf{p}}(t+dt) = \dot{\mathbf{p}}(t) + \beta\frac{dt}{2}(\ddot{\mathbf{p}}(t) + \ddot{\mathbf{p}}(t+dt)), \tag{2}$$

with:

- t the time and dt the time step;
- $\mathbf{p}$, $\dot{\mathbf{p}}$, $\ddot{\mathbf{p}}$ respectively the position vector, the velocity vector and the acceleration vector of one discrete element;
- β the damping coefficient. A value greater than one produces some numerical damping. This coefficient is set to one (no numerical damping) in this paper.

Position and velocity are calculated using the acceleration determined by Newton's second law of motion (see Table 1). The mass of each element is calculated to equalize the mass of the equivalent domain. The continuous domain is defined as the bounding volume of the discrete sample. Linear positions and orientations are respectively associated with resultant forces and torques. Quaternions are used for elements rotations instead of Euler angles so that it follows the same equations as 1 and 2, replacing the position, velocity and acceleration vectors $\mathbf{p}$, $\dot{\mathbf{p}}$, $\ddot{\mathbf{p}}$ by the quaternion ones $\mathbf{q}$, $\dot{\mathbf{q}}$, $\ddot{\mathbf{q}}$.

Table 1 Application of the *velocity Verlet* integration scheme to compute linear positions and translational velocities of one discrete element (DE)

Require: $\mathbf{p}(0)$, $\dot{\mathbf{p}}(0)$, $\ddot{\mathbf{p}}(0)$
$t \leftarrow 0$
for all iteration n **do**
  for all discrete element i **do**
    $\mathbf{p_i}(t+dt) \leftarrow$ Vector position computed from Eq. (1)
    $\mathbf{f_i}(t+dt) \leftarrow$ Balance of forces acting on i
    $\ddot{\mathbf{p}}_\mathbf{i}(t+dt) \leftarrow$ Application of Newton's first law
    $\dot{\mathbf{p}}_\mathbf{i}(t+dt) \leftarrow$ Velocity vector computed from Eq. (2)
  end for $t \leftarrow t+dt$
end for

Discrete elements can interact only by contact or can be connected by cohesive links like springs or 3D beams. As established in André et al. (2012), DEM models using cohesive beams to link discrete elements are appropriate to model continuous materials. All of the deformation modes of the beam have to be taken into account: traction, compression, bending and torsion. The analytical model of the Euler-Bernoulli beam is used to compute the force and torques reactions acting on two discrete elements linked by a beam, see Eqs. 3, 4, 5 and 6. Random compact packing of discrete elements are generated. A beam is assigned for each element in contact creating a random lattice. In this paper the DEM is only used as a lattice approach while offering the possibility in the future to take into account the contacts between the elements.

$$\mathbf{F}_{B/DE_1} = +E_\mu S_\mu \frac{\Delta l_\mu}{l_\mu}\mathbf{X} - \frac{6E_\mu I_\mu}{l_\mu^2}\left((\theta_{2z}+\theta_{1z})\mathbf{Y} + (\theta_{2y}+\theta_{1y})\mathbf{Z}\right) \tag{3}$$

$$\mathbf{F}_{B/DE_2} = -E_\mu S_\mu \frac{\Delta l_\mu}{l_\mu}\mathbf{X} + \frac{6E_\mu I_\mu}{l_\mu^2}\left((\theta_{2z}+\theta_{1z})\mathbf{Y} - (\theta_{2y}+\theta_{1y})\mathbf{Z}\right) \tag{4}$$

Discrete elements can interact only by contact or can be connected by cohesive links like springs or 3D beams. As established in André et al. (2012), DEM models using cohesive beams to link discrete elements are appropriate to model continuous materials. All of the deformation modes of the beam have to be taken into account: traction, compression, bending and torsion. The analytical model of the Euler-Bernoulli beam is used to compute the force and torques reactions acting on two discrete elements linked by a beam, see Eqs. 3, 4, 5 and 6. Random compact packing of discrete elements are generated. A beam is assigned for each element in contact creating a random lattice. In this paper the DEM is only used as a lattice approach while offering the possibility in the future to take into account the contacts between the elements.

$$\mathbf{T}_{B/DE_1} = +\frac{G_\mu I_{0\mu}}{l_\mu}(\theta_{2x} - \theta_{1x})\mathbf{X} \quad (5)$$
$$-\frac{2E_\mu I_\mu}{l_\mu}\left((\theta_{2y} + 2\theta_{1y})\mathbf{Y} - (\theta_{2z} + 2\theta_{1z})\mathbf{Z}\right)$$
$$\mathbf{T}_{B/DE_2} = -\frac{G_\mu I_{0\mu}}{l_\mu}(\theta_{2x} - \theta_{1x})\mathbf{X} \quad (6)$$
$$-\frac{2E_\mu I_\mu}{l_\mu}\left((2\theta_{2y} + \theta_{1y})\mathbf{Y} - (2\theta_{2z} + \theta_{1z})\mathbf{Z}\right)$$

with:

- $\mathbf{F_{B/DE_1}}$ the interaction force of the beam on element 1
- $\mathbf{F_{B/DE_2}}$ the interaction force of the beam on element 2
- $\mathbf{T_{B/DE_1}}$ the interaction moment of the beam on discrete element 1
- $\mathbf{T_{B/DE_2}}$ the interaction moment of the beam on discrete element 2
- l_μ the initial length of the beam
- Δl_μ the elongation of the beam
- $\boldsymbol{\theta_1}$ the rotation vector of the cross section at point O_1
- $\boldsymbol{\theta_2}$ the rotation vector of the cross section at point O_2
- S_μ the cross section area of the beam
- $I_{0\mu}$ the polar moment of inertia of the beam
- I_μ the second moment of inertia in bending of the beam ($I_y = I_z$)
- E_μ Young's modulus of the beam
- G_μ the shear modulus of the beam

It is then possible to create geometries made of discrete elements (see an example in Fig. 2). The work in André et al. (2012) gives the calibration methodology to find the microscopic parameters (i.e. physical parameters of cohesive beams) of the model for a given material. In appendix A, this methodology is applied for a material with a Young's modulus of 10 GPa and a Poisson ratio of 0.3. Microscopic parameters are then find equal to:

- Micro-Young modulus = 356 Gpa;
- Micro-Poisson ratio = 0.3;
- Micro-radius ratio = 0.3.

The DEM is therefore used to extract material parameters from experimental tests by removing the beams manually, which corresponds to the *node release technique*.

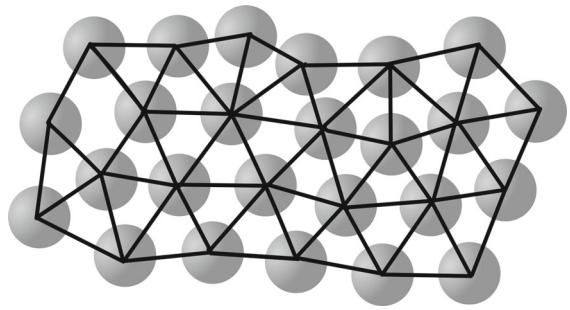

Fig. 2 Discrete elements-lattice structure

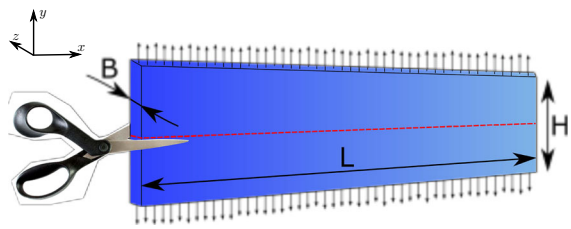

Fig. 3 Geometry of the discrete element plate

2.2 Geometry and boundary condition of the model

The numerical specimen is a plate with a length L of 200 mm, a height H of 40 mm and a thickness B of 2 mm (Fig. 3). The plate contains 20,000 discrete elements with 2 elements in the thickness. Three discrete elements specimens were created to take into account the dispersion of the results due to the random packing. As it was noticed, differences between the 3 specimens were negligible and only the results for one geometry will be presented for clarity.

The pre-stress of the plate is made by imposing an arbitrary displacement of 2 mm in the y-direction on the top boundary condition while the bottom is clamped. The displacement is gradually increased during 20,000 iterations to avoid dynamic effects since no mass scaling technique was used. The plate is then stabilized during 10,000 iterations, which ensures that the residual kinetic energy is negligible. Inertia effects due to the loading represent less than 1% of the total energy and are numerically damped in the pre-stressed phase (the damping is then removed during the dynamic fracture). This procedure allows a quasi-static state of the specimen before fracture. To simulate the opening of the crack, beams are successively disabled between each time step according to the desired crack tip velocity. This process is called in this paper the Simple Node Release Technique (S-NRT). Figure 4 represents a dis-

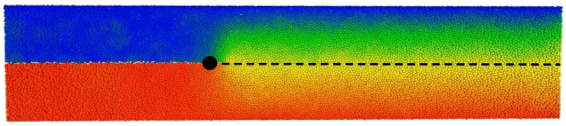

Fig. 4 Dynamic crack propagation in a discrete element plate (discrete elements are coloured depending on their vertical displacement). The dark dot represents the crack tip

crete element plate where a crack propagates along the x axis.

2.3 Energy balance in DEM

The energy release rate is computed by assuming the Linear Elastic Fracture Mechanics (LEFM): non linear effects (such as viscolelasticity) are not considered in the model. The dynamic energy release rate is computed assuming a Griffith energy balance so that:

$$G_{ID} = \frac{\Delta W_{ext} - \Delta W_{elas} - \Delta W_{diss} - \Delta K_{cin}}{2b\Delta a}, \quad (7)$$

where ΔW_{elas} is the increment of elastic energy, ΔK_{cin} is the increment of kinetic energy, ΔW_{ext} is the increment of the work done by external forces and ΔW_{diss} is the increment of dissipated energy (other than the fracture energy) which is null in our case. The increment of projected fracture surface is $2b\Delta a$ with b the width and a the length of the crack. A virtual surface is assumed since the true surface in DEM is not relevant. The virtual surface represents the bounding surface of the crack. The kinetic energy is calculated by adding the kinetic energy of the discrete element i in the simulation ($K^i_{cin} = 1/2 m_i ||\dot{\mathbf{p}}_i||^2$). The elastic energy is calculated by summing the elastic energy of each beam. The elastic energy of each beam is the sum of the beam works of the bending torques, normal forces and torsion torques. The work done by the resultant forces and the moments are taken into account. The integration of the force-displacement curves applied on the boundary conditions allows for finding the work done by external forces.

The energy balance in Fig. 5 illustrates the three phases for the dynamic fracture of a plate: tension (0–0.47 ms), stabilization (0.47–0.71 ms) and fracture (0.71–1.16 ms). The increase of the fracture energy and kinetic energy counterbalanced by a decrease of elastic energy is shown. In the following, the study of the crack tip velocity is presented.

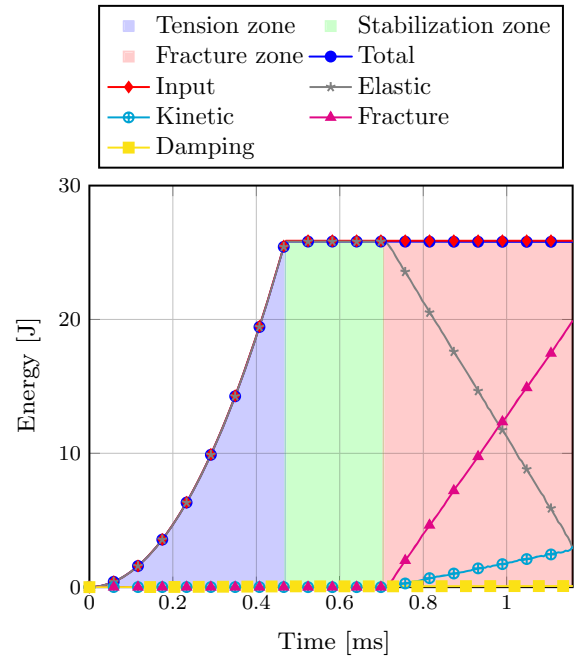

Fig. 5 Energy balance of a plate subjected to dynamic fracture ($\dot{a}/c_r = 0.2$)

2.4 Comparison with semi-infinite plate solution

An analytical solution of a crack propagation in a semi-infinite plate is proposed in Broberg (1960) and is used to validate by comparison the numerical results. In our case, the plate is finite so, in order to avoid dynamic wave reflection effects that are not taken into account in the Broberg solution, the energy analysis is performed only on the early stage of the crack propagation where the fracture energy keeps increasing linearly. Indeed, the semi-infinite plate involves a non-saturation of the fracture energy all along the crack path. Nevertheless, the ratio between the dynamic energy release rate and the quasi-static one reaches a threshold as can be observed with the DEM results in Fig. 6.

3 Simple node release technique (S-NRT)

3.1 First results

The Rayleigh wave speed of the material (c_r) is set in this case to 2200 $m\,s^{-1}$. The results are presented in term of the dynamic correction factor G_{ID}/G_{I0} as a function of the normalized advance of the crack tip for different crack tip velocities in Fig. 6. It appears that a quasi constant energy release rate can be obtained

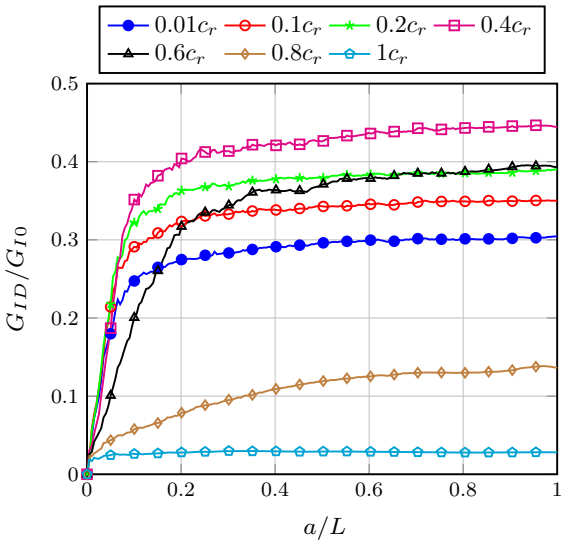

Fig. 6 Dynamic correction factor as a function of the crack tip position for different crack tip velocities using the simple node release technique

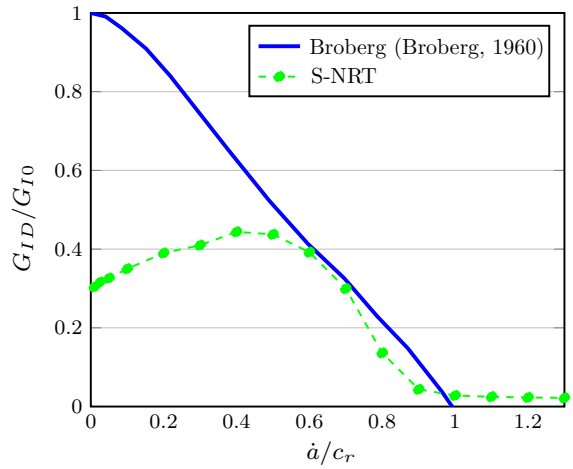

Fig. 7 Dynamic correction factor for a discrete elements plate using the simple node release technique

for most of the crack tip velocities after an advance of the crack of 20 % of the sample length. The assumption that the crack propagates in a semi infinite media can be made for a maximum crack propagation distance. The dynamic correction factor tends to be zero at a crack tip velocity equal to the Rayleigh wave speed.

Figure 7 shows the dynamic correction factor G_{ID}/G_{I0} as a function of the normalized crack tip velocity and makes a comparison with analytical results. Values for the dynamic correction factor are taken from Fig. 6 for each crack tip velocity. The results are in good agreement only between $0.6\,c_r$ and $1\,c_r$. At low crack tip velocity ($0.01\,c_r$), the dynamic correction factor is less than 0.4, far from the analytical value which is close to 1. The current S-NRT approach produces dynamic instabilities, even at low crack tip velocities. A brutal beam deactivation induces oscillations near the crack tip that propagate in all the specimen. This node release technique is not adapted for the simulation of the dynamic fracture.

3.2 Adding damping effects

To reduce dynamic instabilities, a viscous damping is added to the numerical model. The damping acts between each interaction and is expressed as a ratio of the critical damping coefficient α contained in [0, 1]. A force is added for each interaction that takes into account the damping and is equal to:

$$\mathbf{f} = \dot{\delta}\alpha 2\sqrt{KM}\mathbf{n}, \tag{8}$$

with:

- α the damping coefficient,
- $\dot{\delta}$ the relative velocity between two elements connected by a beam,
- K the interaction generalized stiffness,
- M the equivalent mass of the two elements,
- $\mathbf{n}$ the direction of the interaction.

The energy release rate G_I is then updated by incorporating the energy dissipated by the damping.

Two solutions have been tested:

- The damped beams are located only near the crack surface. Less than 6 % of the beams are damped in this case and $\alpha = 0.001$;
- All the beams in the specimen are damped and $\alpha = 0.0002$.

The damping coefficients are so small that they have almost no effect on the behaviour of the structure except when fracture occurs. Indeed, with such small coefficients, only high frequency oscillations close to the highest eigenvalue (two discrete elements in oscillation) are damped. Results with the two solutions are presented in Fig. 8 and are compared with the S-NRT without damping.

Both results obtained with the damping are closer to the analytical value than without damping and present a similar response: undervaluation of the dynamic correction factor from $0.01\,c_r$ to $0.4\,c_r$ and overvaluation

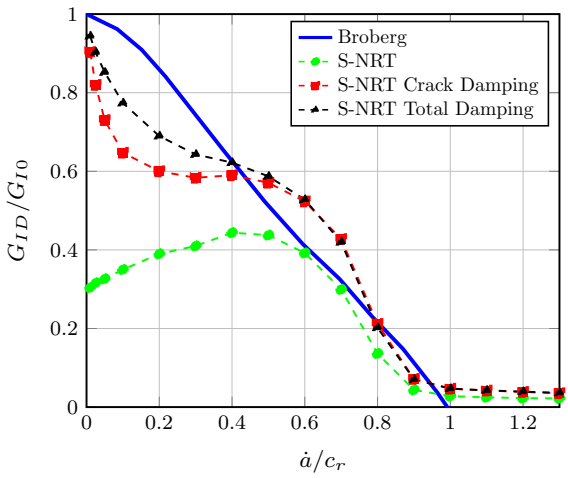

Fig. 8 Dynamic correction factor for a discrete elements plate using the simple node release technique with damped beams only at the crack surface or in the entire specimen

from $0.4\,c_r$ to $0.8\,c_r$. Between $0.01\,c_r$ and $0.4\,c_r$, the second solution (total damping) offers better results. The damping solution has the drawback of slightly changing the behaviour of the structure. A progressive node release technique has to be considered.

4 Progressive node release technique (P-NRT)

4.1 Elasto-damage zone model

The progressive zone release technique is based on the elasto-damage zone model, widely used in FEM (Hsu and Zhai 1984; Kostylev and Margolin 1990). Figure 9 presents a crack propagation in a discrete domain. Ahead of the crack tip, beams are purely elastic (undamaged). Between the traction free zone and the undamaged zone, the damage zone is implemented. In this volume, beams progressively lose their stiffness until their current Young's modulus reaches 0. Young's modulus is associated with the beam kinematic: tension, compression, bending, torsion and shear. Two main parameters have to be identified: the damage zone length and the relaxation scheme of the beams. As it was established in FEM for the node release technique, the relaxation scheme can be linear (Kobayashi et al. 1977) or non linear (Malluck and King 1980; Rydholm et al. 1978) along the damage zone (Fig. 10).

To cover a wide range of solutions, three relaxation schemes were considered (see Eqs. 9, 10 and 11):

$$Y_1/Y_2 = 1 - b/l, \tag{9}$$

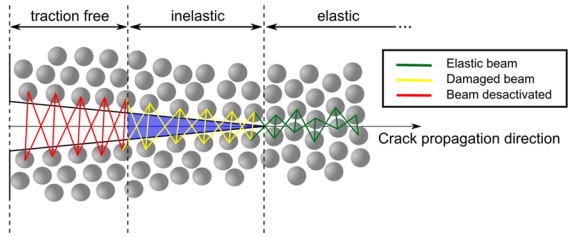

Fig. 9 Representation of the damage zone model

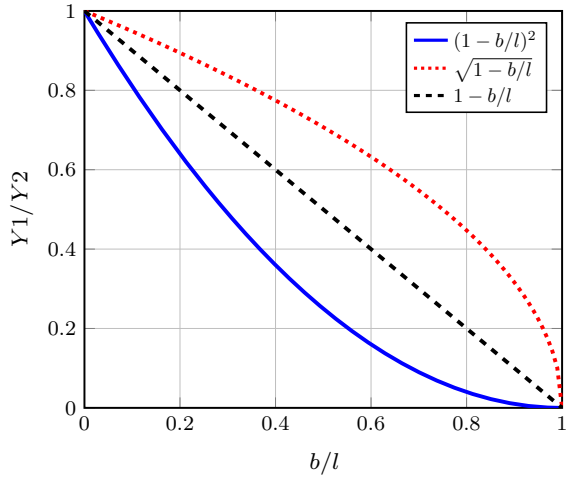

Fig. 10 Relaxation schemes of the damage zone model

$$Y_1/Y_2 = \sqrt{1 - b/l}, \tag{10}$$

$$Y_1/Y_2 = (1 - b/l)^2, \tag{11}$$

with:

- Y_1 Young's modulus at the current time step,
- Y_2 initial Young's modulus,
- l the damage zone length,
- b the distance between the beam considered and the beginning of the damage zone.

The length of the damage zone is normalized with respect to the mean discrete element radius: the ratio $r_l = L_{CZM}/R_{DE}$ is adopted with L_{CZM} the damage zone length and R_{DE} the mean radius in the DEM model.

4.2 Parameter identification of the damage zone model

Figure 11 compares the correction factor using the three different relaxation schemes. A quadratic or linear decay of Young's Modulus makes it possible to obtain a

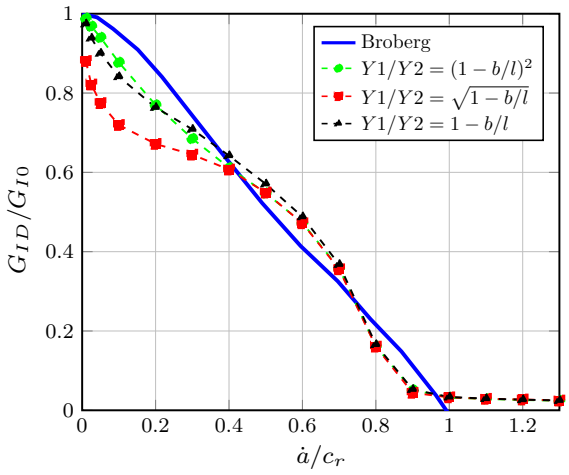

Fig. 11 Comparison of the dynamic correction factor for different relaxation schemes with $L_{CZM}/R_{DE} = 1.0$

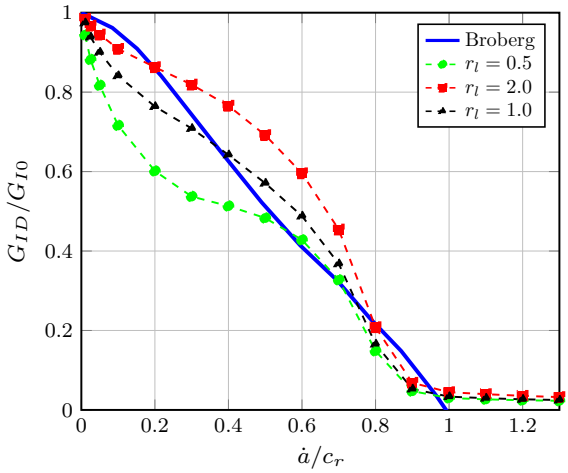

Fig. 12 Comparison of the dynamic correction factor for different lengths of the damage zone with a linear relaxation scheme ($Y1/Y2 = 1 - b/l$)

result close to the analytical solution. The third scheme, which results in more rigid beams at the damage zone, does not allow the model to dissipate enough fracture energy at crack propagation rates of $0.05\,c_r$ to $0.4\,c_r$. The linear relaxation scheme is finally retained, as recommended in Aoki et al. (1987) for the FEM.

The damage zone length L_{CZM} is compared in Fig. 12. A length equivalent to the ratio $r_l = 1$ offers the best results. A longer length ($r_l = 1.5$) leads to

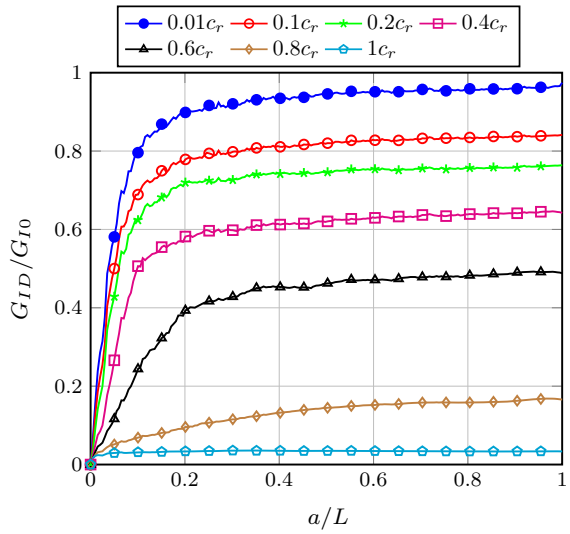

Fig. 13 Dynamic correction factor as a function of the crack tip position for different crack tip velocities using the progressive node release technique

energy dissipated by too high fractures (between $0.2\,c_r$ and $0.8\,c_r$) while a shorter length ($r_l = 0.5$) underestimates the fracture energy (between $0.01\,c_r$ and $0.6\,c_r$). In the case of the model presented here, the damage zone has a length of 0.49 mm which is approximately 0.0024 times the length of the plate. At $0.1\,c_r$, a beam takes about 100 time steps to degrade and 10 time steps at $1\,c_r$. The decrease of the time step did not show any influence on the results.

Figure 13 presents the results with the dynamic correction factor as a function of the normalized advance of the crack tip for the P-NRT with the two identified parameters. Results are in good agreement with the analytical data compared to the S-NRT (Fig. 6). As expected, at $0.01\,c_r$, the dynamic correction factor tends to 1. A constant energy release rate is reached between 10 % and 20 % of the normalized advance of the crack tip for most of the crack tip velocities. High velocities (more than $0.8\,c_r$) require about 40 % of the normalized advance of the crack tip. The geometry is adapted to the problem and a longer plate will not offer better results since a constant energy release rate is reached.

In order to validate the parameters found for different geometries, plates were created with an increasing number of discrete elements. Two elements were kept

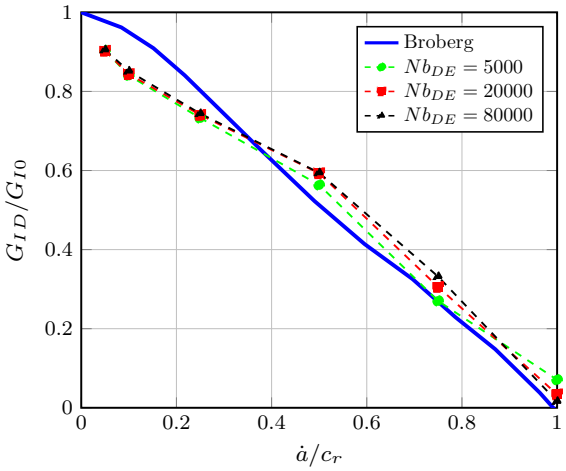

Fig. 14 Influence of the number of discrete element in the simulation by keeping 2 elements in the thickness of the plate

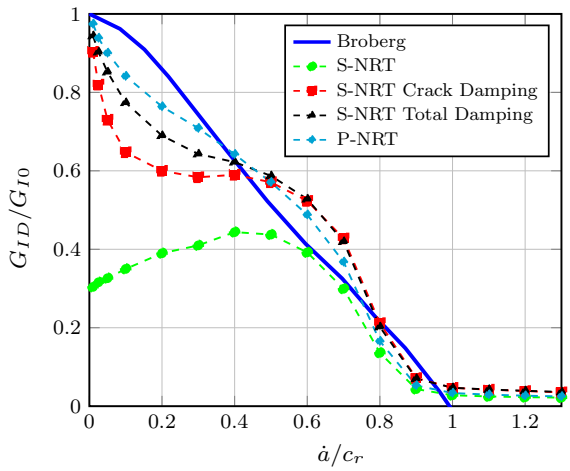

Fig. 15 Comparison of the dynamic correction factor for different release node techniques in DEM

in the thickness to have the same arrangement of elements in the plate. The Fig. 14 presents the dynamic correction factor as a function of the crack tip velocity for 5000, 20,000 and 80,000 elements in the numerical specimen. As it can be seen, the number of element has almost no influence on the results, especially between 20,000 and 80,000 elements. For these two specimens, a difference $\Delta\left(G_{ID}/G_{I0}\right) \approx 0.002$ is measured at $0.05\,c_r$ and a difference $\Delta\left(G_{ID}/G_{I0}\right) \approx 0.018$ is measured at $1\,c_r$.

5 Discussion and conclusions

Numerical models using the DEM have been implemented to study the dynamic fracture and were compared with analytical results found in Broberg (1960). The dynamic correction factor was calculated for cracks running in a pre-stressed plate. A numerical node release technique is proposed with two different methods: a simple and a progressive release technique. It has been shown that the S-NRT generates dynamic instabilities (underestimation of the dynamic correction factor) that can be corrected by adding numerical damping. Using damped beams in all the numerical specimen offers better results than using damped beams only near the crack surfaces. A damage zone is inserted for the second method where the Young's modulus of the beams are progressively lowered. A linear degradation scheme coupled to a ratio of the damage zone length of 1 allows to reproduce the results obtained analytically with more accuracy and no damping at all (see Fig. 15). However, the quasi-linear result expected for the dynamic correction factor is not obtained. The models fail to dissipate enough fracture energy below $0.4\,c_r$.

It can also be noted in Fig. 15 that the dynamic correction factor tends to 1 and 0 as a function of the crack tip velocity without reaching these limits. At low velocity, it can be explained by the presence of residual inertial effects due to the explicit time integration scheme. The beams are not aligned at the the crack tip, which leads to slight normal perturbations to the plate causing bending oscillations of the plate. At a velocity close to $1\,c_r$, a dynamic correction factor greater than 0 is due to the fact that there is no special treatment of the geometric singularity of the crack tip: the broken beams possess a minimum of elastic energy corresponding to a part of the energy stored by the pre-stress of the plate. An increase in the number of elements causes a tendency towards 0.

In the future, the nodal release technique in DEM will allow us to explore different situations by taking into account contact and friction at the crack surfaces which can occur for mode II and mode III crack problems. The propagation of curvilinear cracks can be studied easily. One DEM specimen is suitable for many crack paths (rectilinear or more complex) because the crack paths are independent of the discrete elements

arrangement in contrast to the mesh in the FEM. Eventually, the next step is to use the critical energy release rate calculated from the DEM and the experimental data to serve a DEM *application phase simulation*.

Acknowledgements This work was carried out in the frame of the FUI project SAMBA funded by BPI, région Midi-Pyrénées, région Aquitaine and approved by the Aerospace Valley. The SAMBA project, (for Shock Absorber Material for Birdshield Application), backed by STELIA Design and Research Division, concerns the development of new generation bird impact shields for commercial and business aircraft. The authors gratefully acknowledge the members of the project: STELIA (AirbusGroup), CEDREM, ESTEVE, NIMITECH, HUTCHINSON, Institut Clément Ader and ATECA SAS. The authors would also like to show their gratitude to Christophe Fond, Professor at the University of Strasbourg for sharing his expertise on dynamic fracture.

Compliance with ethical standards

Conflict of interest The authors declare that there are no conflicts of interest regarding the publication of this paper.

Disclosure Part of this work was presented at the Fifth International Conference on Computational Modeling of Fracture and Failure of Materials and Structures (2017) in Nantes, France.

Appendix: Elastic calibration

The first step in the elastic calibration is to ensure that the discrete meshing is fine enough to retrieve the macroscopic elastic properties obtained experimentally. The numerical convergence is assumed when the macroscopic parameters such as Young's modulus and the Poisson ratio converge to one value, Fig. 17. To achieve this convergence, several discrete cylindrical domains from 500 to 35,000 elements were created, see in Fig. 16. Each of them was generated five times in order to use the average for each discrete domain refinement and to quantify the dispersion.

A numerical compressive test on each specimen is then performed. A load force is imposed on each side of the cylinder (on each center of elements belonging respectively to the top and bottom set of the cylinder), progressively applied and stabilized. Only elastic properties of the model are investigated so plates are not simulated and friction between the plates and the cylinder is not considered. The rate of loading forces is chosen to ensure a quasi-static solicitation and therefore to have a negligible kinetic energy compared to the total energy. Young's macroscopic modulus and the Poisson ratio are estimated knowing the force applied at the top and bottom and the change in length and radius of the cylinder. According to the two top charts in Fig. 17, a discrete element number greater than 15,000 is found to converge: Young's modulus and Poisson ratio values are within ±2.5 %. Microscopic parameters are scanned, interpolated and finally selected, see the two bottom charts in Fig. 17 and Table 2.

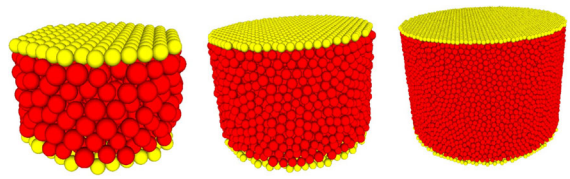

Fig. 16 Cylindrical DEM geometries with three levels of refinement: 750, 5500 and 35,000 elements

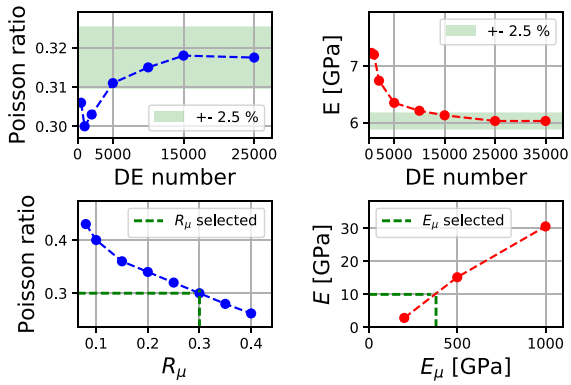

Fig. 17 Elastic calibration

Table 2 Macroscopic and microscopic elastic parameters

	Young's modulus	Poisson ratio	Radius ratio
Macroscopic	$E_M = 10.3\ GPa$	$\nu_M = 0.3$	None
Microscopic	$E_\mu = 356\ GPa$	$\nu_\mu = 0.3$	$R_\mu = 0.3$

References

Andre D, Charles J-L, Iordanoff I, Néauport J (2014) The granoo workbench, a new tool for developing discrete element sim-

ulations, and its application to tribological problems. Adv Eng Softw 74:40–48
André D, Iordanoff I, Charles J-L, Néauport J (2012) Discrete element method to simulate continuous material by using the cohesive beam model. Comput Methods Appl Mech Eng 213:113–125
André D, Jebahi M, Iordanoff I, Charles J-L, Néauport J (2013) Using the discrete element method to simulate brittle fracture in the indentation of a silica glass with a blunt indenter. Comput Methods Appl Mech Eng 265:136–147
Aoki S, Kishimoto K, Sakata M (1987) Finite element computation of dynamic stress intensity factor for a rapidly propagating crack using j-integral. Comput Mech 2(1):54–62
Brabel B (2007) Modélisation avec la méthode X-FEM de la propagation dynamique et de l'arret de fissure de clivage dans un acier de cuve REP. Thèse, Institut National des Sciences Appliquées de Lyon
Broberg KB (1960) The propagation of a brittle crack. Arkiv Fysik 18(2):159–192
Cundall PA, Strack OD (1979) A discrete numerical model for granular assemblies. Geotechnique 29(1):47–65
Delaplace A, Desmorat R (2008) Discrete 3d model as complimentary numerical testing for anisotropic damage. Int J Fract 148(2):115
Delaplace A, Ibrahimbegovic A (2003) Discrete modeling of cracking of brittle materials in large relative motion and localization problem, pp 375–383. Springer, Netherlands
Egholm DL (2007) A new strategy for discrete element numerical models: 1. theory. J Geophys Res: Solid Earth 112(B5)
Fakhimi A, Villegas T (2007) Application of dimensional analysis in calibration of a discrete element model for rock deformation and fracture. Rock Mech Rock Eng 40(2):193–211
Fillot N, Iordanoff I, Berthier Y (2007) Modelling third body flows with a discrete element methoda tool for understanding wear with adhesive particles. Tribol Int 40(6):973–981
Granoo's wiki. http://www.granoo.org
Grégoire D (2008) Initiation, propagation, arrêt et redémarrage de fissures sous impact. Thèse, Institut National des Sciences Appliquées de Lyon
Guessasma M, Fortin, J (2011) Modélisation d'un milieu discret cohésif par l'approche dynamique des contacts: application à la rupture d'un matériau cimentaire. In 10e colloque national en calcul des structures, pages Clé–USB
Hedjazi L, Martin C, Guessasma S, Della Valle G, Dendievel R (2012) Application of the discrete element method to crack propagation and crack branching in a vitreous dense biopolymer material. Int J Solids Struct 49(13):1893–1899
Hsu T, Zhai Z (1984) A finite element algorithm for creep crack growth. Eng Fract Mech 20(3):521–533
Jalali P, Hyppänen T (2015) Momentum transport between two granular phases of spherical particles with large size ratio: two-fluid model versus discrete element method. Powder Technol 273:13–18
Kannan K, Kumar RK, Prabhakar O (1993) Finite element crack growth algorithm for dynamic fracture. Comput Mech 12(6):349–359
Kawabata T, Nakanishi D, Namegawa T, Aihara S (2018) Dissipation energy during brittle crack propagation in a single crystal of 3% si-fe alloy. Mater Phys Mech 36(1):18–38
Keegstra P, Head J, Turner C (1978) Numerical methods in fracture mechanics. University College, Swansea, pp 634–647
Kobayashi A, Emery AF, Mall S (1976) Dynamic-finite-element and dynamic-photoelastic analyses of two fracturing homalite-100 plates. Exp Mech 16(9):321–328
Kobayashi A, Mall S, Urabe Y, Emery A (1977) A numerical dynamic fracture analyses of three wedge-loaded dcb specimens. Technical report, DTIC Document
Kopp J-B, Fond C, Hochstetter G (2018) Rapid crack propagation in pa11: an application to pipe structure. Eng Fract Mech
Kopp J-B, Lin J, Schmittbuhl J, Fond C (2014a) Longitudinal dynamic fracture of polymer pipes. Eur J Environ Civ Eng 18(10):1097–1105
Kopp J-B, Schmittbuhl J, Noel O, Lin J, Fond C (2014b) Fluctuations of the dynamic fracture energy values related to the amount of created fracture surface. Eng Fract Mech 126:178–189
Kostylev V, Margolin V (1990) Fem solution of a dynamic elastoplastic problem of fracture mechanics. 2. Supercritical crack propagation. Strength Mater 22(7):943–953
Malluck J, King W (1980) Fast fracture simulated by conventional finite elements: a comparison of two energy-release algorithms. In: Crack arrest methodology and applications. ASTM International
Masurel A (2015) Modélisation mixte éléments discrets/éléments finis de la dégradation de structures en béton armé sous impact sévère. PhD thesis, Université Grenoble Alpes
Menouillard T (2007) Dynamique explicite pour la simulation numérique de propagation de fissure par a méthode des éléments finis étendus. Thèse, Institut National des Sciences Appliquées de Lyon
Nishioka T (1995) Recent developments in computational dynamic fracture mechanics. Dynamic fracture mechanics(A 96–14151 02–39). Southampton, United Kingdom and Billerica, MA, Computational Mechanics Publications 1995:1–60
Nishioka T (1997) Computational dynamic fracture mechanics. Int J Fract 86(1–2):127–159
Nishioka T, Atluri S (1982) Numerical analysis of dynamic crack propagation: generation and prediction studies. Eng Fract Mech 16(3):303–332
Nishioka T, Atluri S (1984) Path-independent integral and moving isoparametric elements for dynamic crack propagation. AIAA J 22(3):409–414
Nishioka T, Atluri SN (1980) Numerical modeling of dynamic crack propagation in finite bodies, by moving singular elementspart 1: formulation. J Appl Mech 47(3):570–576
Nistor I (2005) Identification expérimentale et simulation numérique de l'endommagement en dynamique rapide : application aux structures aéronautiques. Thèse, Institut National Polytechnique de Toulouse
Oliver-Leblond C, Delaplace A, Ragueneau F (2015) Modelling of three-dimensional crack patterns in deep reinforced concrete structures. Eng Struct 83:176–186
Réthoré J (2005) Méthode éléments finis étendus en espace et en temps : Application a la propagation dynamique des fissures. Thèse, Institut National des Sciences Appliquées de Lyon
Rougier E, Munjiza A, John N (2004) Numerical comparison of some explicit time integration schemes used in dem, fem/dem and molecular dynamics. Int J Numer Methods Eng 61(6):856–879

Rydholm G, Fredriksson B, Nilsson F (1978) Numerical methods in fracture mechanics. In: Luxmoore AR, Owen DRJ (eds) University College, Swansea, pp 660–672

Song J-H, Wang H, Belytschko T (2008) A comparative study on finite element methods for dynamic fracture. Comput Mech 42(2):239–250

Swenson D, Ingraffea A (1988) Modeling mixed-mode dynamic crack propagation nsing finite elements: theory and applications. Comput Mech 3(6):381–397

Vassaux M, Oliver-Leblond C, Richard B, Ragueneau F (2016) Beam-particle approach to model cracking and energy dissipation in concrete: Identification strategy and validation. Cem Concr Compos 70:1–14

Yagawa G, Sakai Y, Ando Y (1977) Analysis of a rapidly propagating crack using finite elements. In: Fast fracture and crack arrest. ASTM International

Yanagimoto F, Shibanuma K, Nishioka Y, Shirai Y, Suzuki K, Matsumoto T (2018) Local stress evaluation of rapid crack propagation in finite element analyses. Int J Solids Struct

Zhou F, Molinari J-F, Shioya T (2005) A rate-dependent cohesive model for simulating dynamic crack propagation in brittle materials. Eng Fract Mech 72(9):1383–1410